iScience

CellPress
OPEN ACCESS

Article

Major depression-related factor NEGR1 controls salivary secretion in mouse submandibular glands

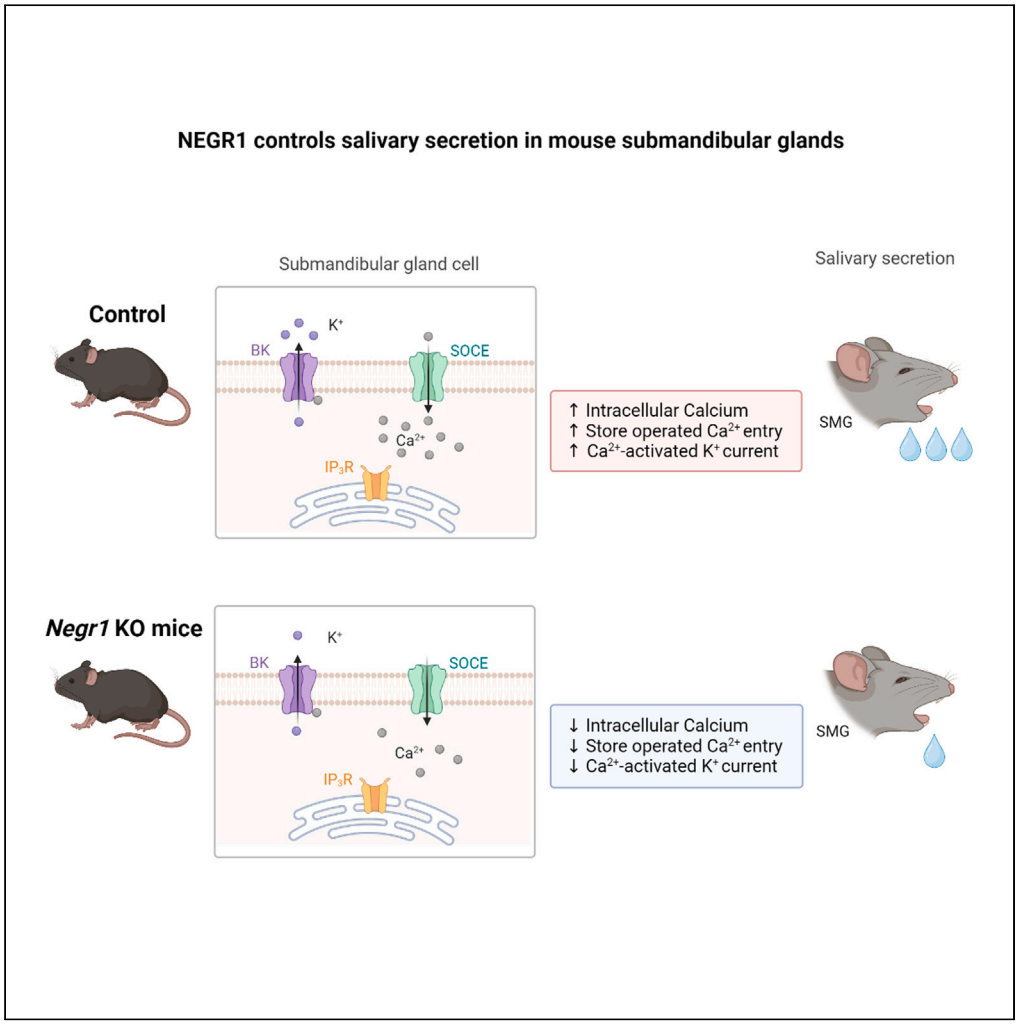

Jisoo Lee, Soohyun Kim, Boram Lee, ..., Woong Sun, Hee-Kyung Park, Se-Young Choi

dentopark@snu.ac.kr (H.-K.P.)
sychoi@snu.ac.kr (S.-Y.C.)

Highlights

Negr1 knockout mice show reduced salivation

NEGR1 is essential for muscarinic Ca^{2+} signaling in the submandibular gland

The study provides an explanation for dry mouth among depression patients

Lee et al., iScience *26*, 106773
May 19, 2023
https://doi.org/10.1016/j.isci.2023.106773

iScience

CellPress
OPEN ACCESS

Article

Major depression-related factor NEGR1 controls salivary secretion in mouse submandibular glands

Jisoo Lee,[1] Soohyun Kim,[1] Boram Lee,[2] Yoo-Bin Kim,[1] Kwang Hwan Kim,[1] Gehoon Chung,[1] Sung Joong Lee,[1] Soojin Lee,[3] Woong Sun,[2] Hee-Kyung Park,[4,*] and Se-Young Choi[1,5,*]

SUMMARY

Salivary gland cells, which secrete water in response to neuronal stimulation, are closely connected to other neurons. Transcriptomic studies show that salivary glands also express some proteins responsible for neuronal function. However, the physiological functions of these common neuro-exocrine factors in salivary glands are largely unknown. Here, we studied the function of Neuronal growth regulator 1 (NEGR1) in the salivary gland cells. NEGR1 was also expressed in mouse and human salivary glands. The structure of salivary glands of *Negr1* knockout (KO) mice was normal. *Negr1* KO mice showed tempered carbachol- or thapsigargin-induced intracellular Ca^{2+} increases and store-operated Ca^{2+} entry. Of interest, the activity of the large-conductance Ca^{2+}-activated K^+ channel (BK channel) was increased, whereas Ca^{2+}-activated Cl^- channel ANO1 channel activity was not altered in *Negr1* KO mice. Pilocarpine- and carbachol-induced salivation was decreased in *Negr1* KO mice. These results suggest that NEGR1 influence salivary secretion though the muscarinic Ca^{2+} signaling.

INTRODUCTION

The functions of the salivary glands are precisely regulated by neuronal signals.[1] Salivary gland cells have muscarinic receptors that recognize acetylcholine secreted from the parasympathetic terminal. Communication between neurons and salivary gland cells consists of neurotransmitter secretions and receptor signaling and occur in a manner similar to signal transduction between neurons.[2] Cell-to-cell communication is a common and important mechanism of various physiological functions. For example, muscarinic receptors, which are important in neuron-to-neuron communication, also play an important role in neuron-to-salivary gland communication. If a factor regulating neuron-to-neuron communication was also expressed in the salivary glands, this factor would play an important role in neuron-to-salivary gland communication in the parasympathetic terminal of the salivary gland.

Recent transcriptomic analyses of salivary glands have revealed many factors linked to salivary gland function.[3–9] These studies have contributed greatly to understanding the differences between the three major salivary glands,[3,4] the diversity of cells constituting salivary glands,[5] and the developmental mechanisms of salivary glands.[4,6,7,9] Notably, many genes (e.g., *Tlx2, Hand2, Phox2b, Ascl1, Tubb4, Sox10*, and *Ngfr*) expressed in the submandibular glands are similarly expressed in neurons.[6,7] In addition, the salivary functions of the factors that have been identified in the neurons have been studied. For example, Rac1/cdc42 and their interactors are important for the structure and function of neuronal synapses.[10] However, the roles of common neuron-salivary gland factors in salivary function remain largely unknown.

Neuronal growth regulator 1 (NEGR1) is a GPI-linked cell-adhesion molecule and a part of the immunoglobulin LON (IgLON) family with Ig-like domains. NEGR1, which was initially discovered as an obesity-related factor,[11–13] is expressed throughout the brain, including in the cerebral cortex and hippocampus.[14] A genome-wide association investigation of major depression revealed that NEGR1 is an etiological factor for major depression.[15–17] NEGR1 plays an important role in synaptic structure and function, including the promotion of synaptogenesis and dendrite formation.[18,19] In addition, NEGR1 regulates receptor signaling in postsynaptic neurons and maintains synaptic plasticity.[20,21] However, the role of NEGR1 expression in the salivary glands has not yet been elucidated.

[1]Department of Physiology, Dental Research Institute, Seoul National University School of Dentistry, Seoul 03080, Republic of Korea

[2]Department of Anatomy, Brain Korea 21 Plus Program for Biomedical Science, Korea University College of Medicine, Seoul 02841, Republic of Korea

[3]Department of Microbiology and Molecular Biology, Chungnam National University, Daejeon 34134, Republic of Korea

[4]Department of Oral Medicine and Oral Diagnosis, Dental Research Institute, Seoul National University School of Dentistry, Seoul 03080, Republic of Korea

[5]Lead contact

*Correspondence: dentopark@snu.ac.kr (H.-K.P.), sychoi@snu.ac.kr (S.-Y.C.)

https://doi.org/10.1016/j.isci.2023.106773

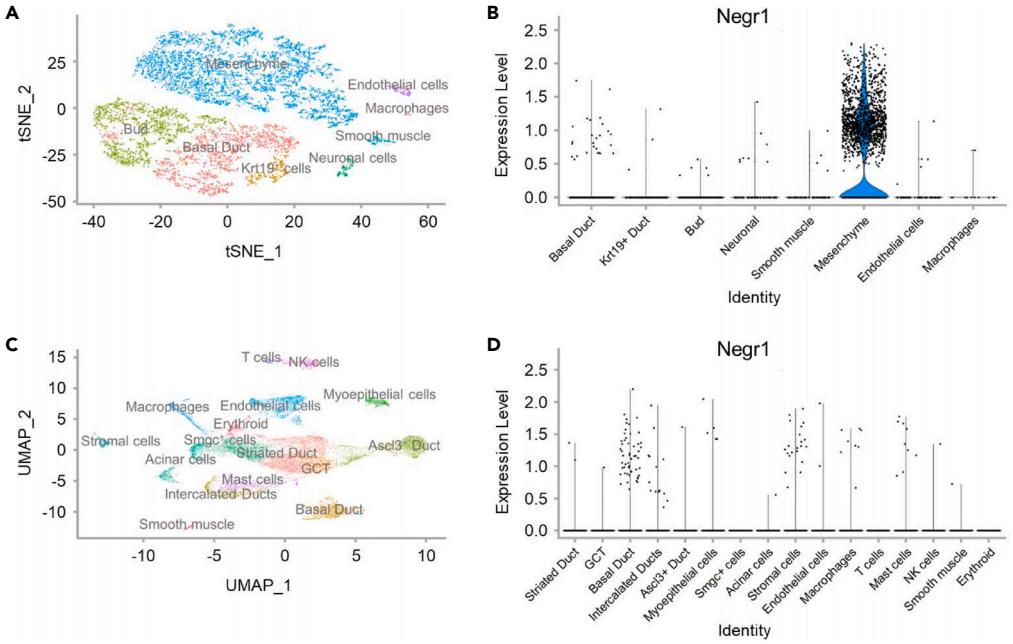

Figure 1. Neuronal growth regulator 1 (*Negr1*) mRNA expression in mouse submandibular gland analyzed by single cell RNA-seq database

(A) tSNE (t-distributed stochastic neighbor embedding) plot of embryonic day 12 (E12) mouse submandibular glands.

(B) Violin plots demonstrate expression of Negr1 in the cell populations of E12 submandibular glands. The single cell RNA-seq datasets can be found in the Gene Expression Omnibus (GEO) database at https://www.ncbi.nlm.nih.gov/geo/-GSE127469.

(C) Uni-form manifold approximation and projection (UMAP) plot of adult mouse submandibular glands.

(D) Violin plots demonstrate expression of Negr1 in the cell populations of adult mouse submandibular glands. The single cell RNA-seq datasets can be found in the GEO database at https://www.ncbi.nlm.nih.gov/geo/- GSE175649.

Here, we tested salivary secretion in an animal model without NEGR1 expression and investigated changes in the cellular mechanism of salivation. We found that NEGR1 is expressed in the salivary glands and plays an important role in maintaining Ca^{2+} signaling of muscarinic receptors. Attempts to elucidate the salivary gland function of common neuro-salivary gland factors can contribute to elucidating the mechanism of dry mouth of unknown cause.

RESULTS

Neuronal growth regulator 1 (*Negr1*) expressed in mouse and human salivary glands

First, we searched the publicly accessible single-cell RNA-seq database to see whether NEGR1 expression could be detected in the mouse submandibular gland. In embryonic day 12 submandibular gland mesenchyme (Figures 1A and 1B) and adult mouse submandibular gland duct (Figures 1C and 1D), NEGR1 expression was confirmed. We sought to confirm that NEGR1 is expressed in the mouse submandibular glands. The polymerase chain reaction (PCR) results showed that NEGR1 is expressed not only in the mouse brain (i.e., the cerebral cortex and hippocampus) and stomach, but also in mouse submandibular salivary glands (Figure 2A). We conducted a quantitative PCR experiment to verify the expression of NEGR1 (Figure 2C). We found that NEGR1 was also expressed in the human submandibular gland by performing RT-PCR on samples of human submandibular gland (HSG) tissue and the HSG cell line (Figure 2B). To reveal the function of NEGR1 in the salivary glands, we examined the structure and function of the salivary glands in knockout (KO) mice in which NEGR1 expression was eliminated. Ultimately, there was no difference in gross morphology (Figure 2D), and the size (Figure 2E) of the submandibular glands between wild-type (WT) mice and *Negr1* KO mice. The expression levels of acinar cell marker aquaporin-5 (AQP5) and ductal cell marker E-cadherin were not altered in *Negr1* KO mice (Figure 2F). Performing immunohistochemical analysis using AQP5 and E-cadherin, we found that *Negr1* KO mice have normal acinar and ductal structures in their submandibular glands. (Figure 2G). Despite being expressed during the embryonic period, these results suggest that NEGR1 does not affect the development of mouse submandibular glands.

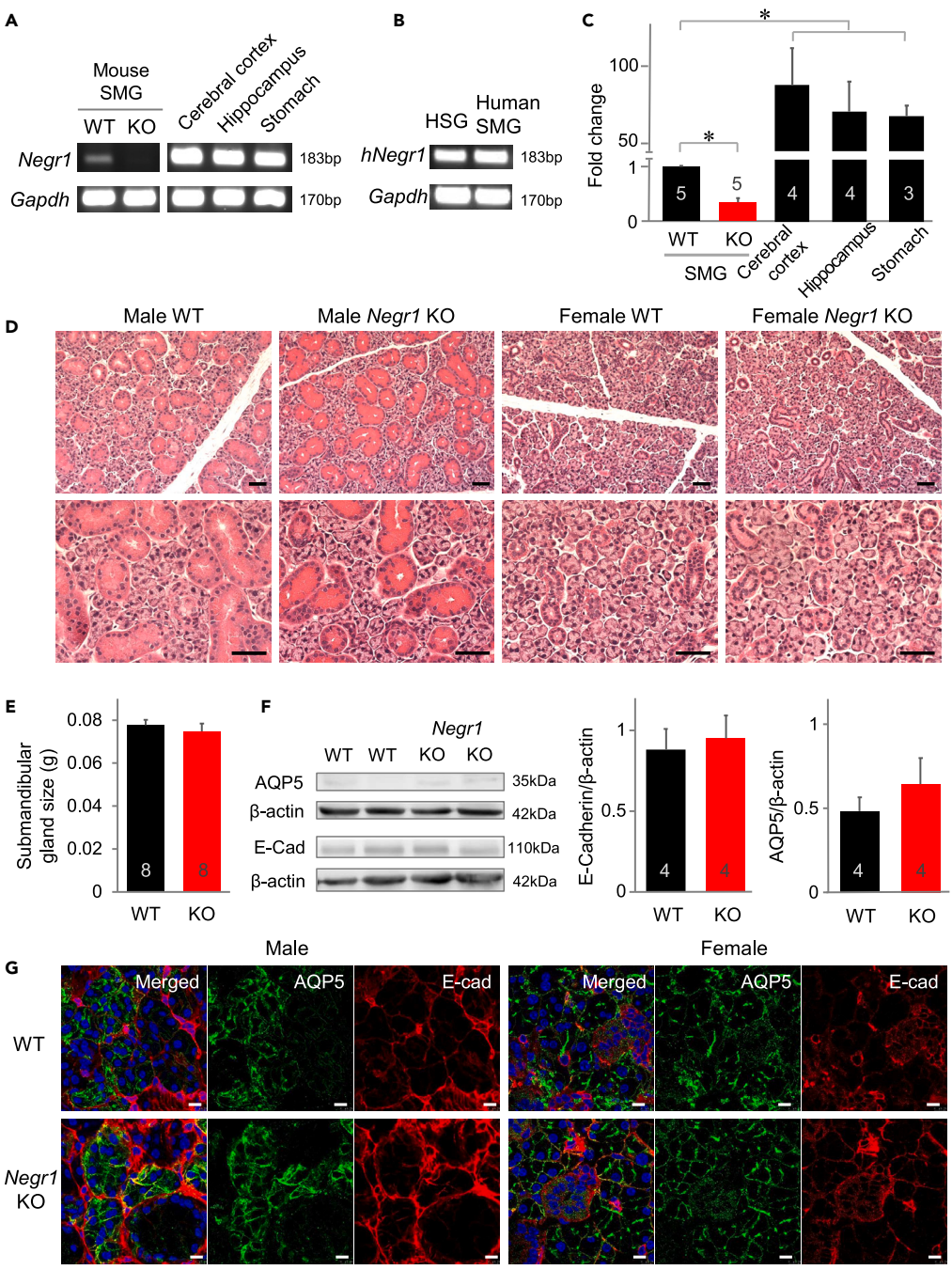

Figure 2. *Negr1* expressed in mouse and human salivary glands

(A) Messenger RNA expression levels of mouse *Negr1* genes were monitored in the mouse submandibular glands, cerebral cortex, hippocampus, and stomach of wildtype (WT) and *Negr1* knockout (KO) mice. *Gapdh*: glyceraldehyde 3-phosphate dehydrogenase, a housekeeping gene used as a PCR positive control.

(B) Messenger RNA expression levels of human *Negr1* genes were monitored in a human submandibular gland (HSG) cell line and human submandibular gland tissue. *Gapdh*: a housekeeping gene used as a PCR positive control.

(C) Quantitative RT-PCR analysis of *Negr1* messenger RNA in the mouse submandibular glands, cerebral cortex, hippocampus, and stomach of WT (n = 5) and *Negr1* KO mice (n = 5) normalized to a reference gene (Gapdh). Fold change in *Negr1* mRNA expression is relative to WT mice and averaged from independent experiments.

(D) The gross morphology of the submandibular gland tissue from WT and *Negr1* KO mice was visualized by hematoxylin and eosin staining. Scale bars, 50 μm.

(E) The submandibular gland size was monitored in WT (n = 8) and *Negr1* KO mice (n = 8).

Figure 2. *Continued*

(F) The expression levels of aquaporin-5 (AQP5) and E-cadherin (E-cad) were monitored in the submandibular gland of WT (n = 4) and *Negr1* KO mice (n = 4).

(G) Representative immunofluorescence images of mouse submandibular gland tissues were immunostained with anti-AQP5 (green) and anti-E-cadherin (red), and merged with DAPI image (blue). Scale bar, 10 μm. Data are represented as mean ± SEM. *p < 0.05.

Negr1 expression is not related in primary Sjogren's syndrome

Because Sjogren's syndrome is one of the main causes of dry mouth, it is interesting to examine the correlation between NEGR1 and Sjogren's syndrome. We found two databases by searching the NCBI GEO database with the keyword 'Sjogren' (GEO: GSE164885, GEO: GSE135635), although there were no results with the keyword 'dry mouth' or 'xerostomia'. A study targeting plasmacytoid dendritic cells and the expression of NEGR1 revealed fold changes of 1.14 and 0.89 in primary Sjogren syndrome patients compared to healthy donors[22] (Figure 3A). Another study targeting peripheral blood mononuclear cells showed that the expression of NEGR1 had a fold change of 1.24 in primary Sjogren's syndrome patients compared to healthy donors[23] (Figure 3B). This means that NEGR1 expression does not show significant changes in Sjogren's syndrome.

AQP5 expression is not altered in *Negr1* KO mice

We also evaluated the effects of NEGR1 on the expression of AQP5, which allows water movement and saliva formation. The total messenger RNA expression of AQP5 in the submandibular glands confirmed by quantitative PCR did not differ between the two types of mice (Figures 4A and 4B). We performed AQP5 FACS analysis with EpCAM, an epithelial cell adhesion molecule, and found that there was no difference in the AQP5 surface expression levels between WT and *Negr1* KO mice (Figures 4C–4E).

Muscarinic Ca^{2+} signaling and store-operated Ca^{2+} entry are decreased in *Negr1* KO mouse

To investigate the molecular mechanism of reduced salivation in *Negr1* KO mice, we examined muscarinic Ca^{2+} signaling, which plays an important role in salivary secretion. We found that the carbachol-mediated intracellular Ca^{2+} increase was smaller in *Negr1* KO mice than in WT mice (Figures 5A–5C). Activation of muscarinic receptors in the salivary glands triggers a release of Ca^{2+} from the intracellular calcium pool via phospholipase C (PLC)-mediated inositol 1,4,5-trisphospate (IP_3) production, which is followed up by

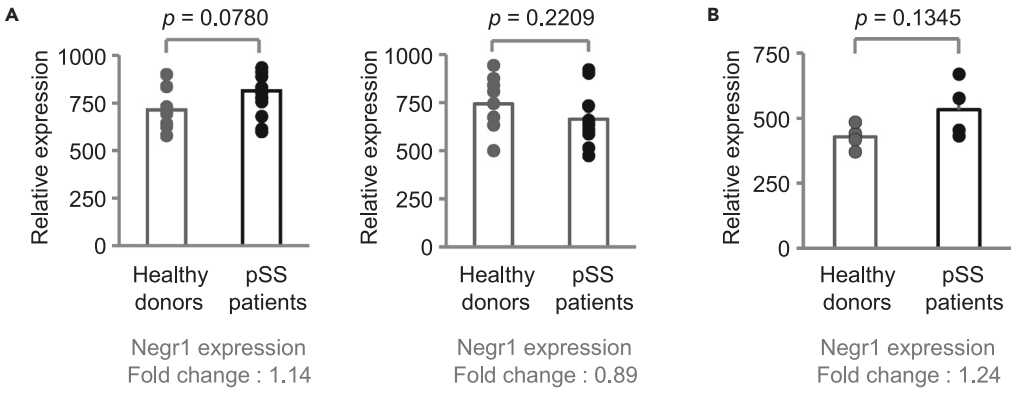

Figure 3. Negr1 mRNA expression in healthy donors and patients with primary Sjogren's syndrome

(A) The bar graph indicates the relative expressions of Negr1 mRNA levels in healthy donors and patients. Publicly available RNA-seq data of plasmacytoid dendritic cells (pDC) from healthy donors and patients with primary Sjogren's syndrome (pSS) were used. This study included two independent cohorts of donors and patients (n = 31 for each group) and we performed RNA-seq with different sequencers (*left*: NextSeq 500 sequencer; *right*: Illumina HiSeq 4000 sequencer). The RNA-seq datasets can be found in the GEO database at https://www.ncbi.nlm.nih.gov/geo/-GSE135635.

(B) The bar graph indicates the relative expressions of Negr1 mRNA levels in healthy donors and patients with pSS. Publicly available RNA-seq data[2] of peripheral blood mononuclear cells (PBMCs) from healthy donors and pSS patients were used (n = 4 per group). This study analyzed the mRNA expression profiles in the PBMCs of healthy donors and patients with pSS using transcription sequencing. The RNA-seq datasets can be found in the GEO database at https://www.ncbi.nlm.nih.gov/geo/- GSE164885. Data are represented as mean ± SEM.

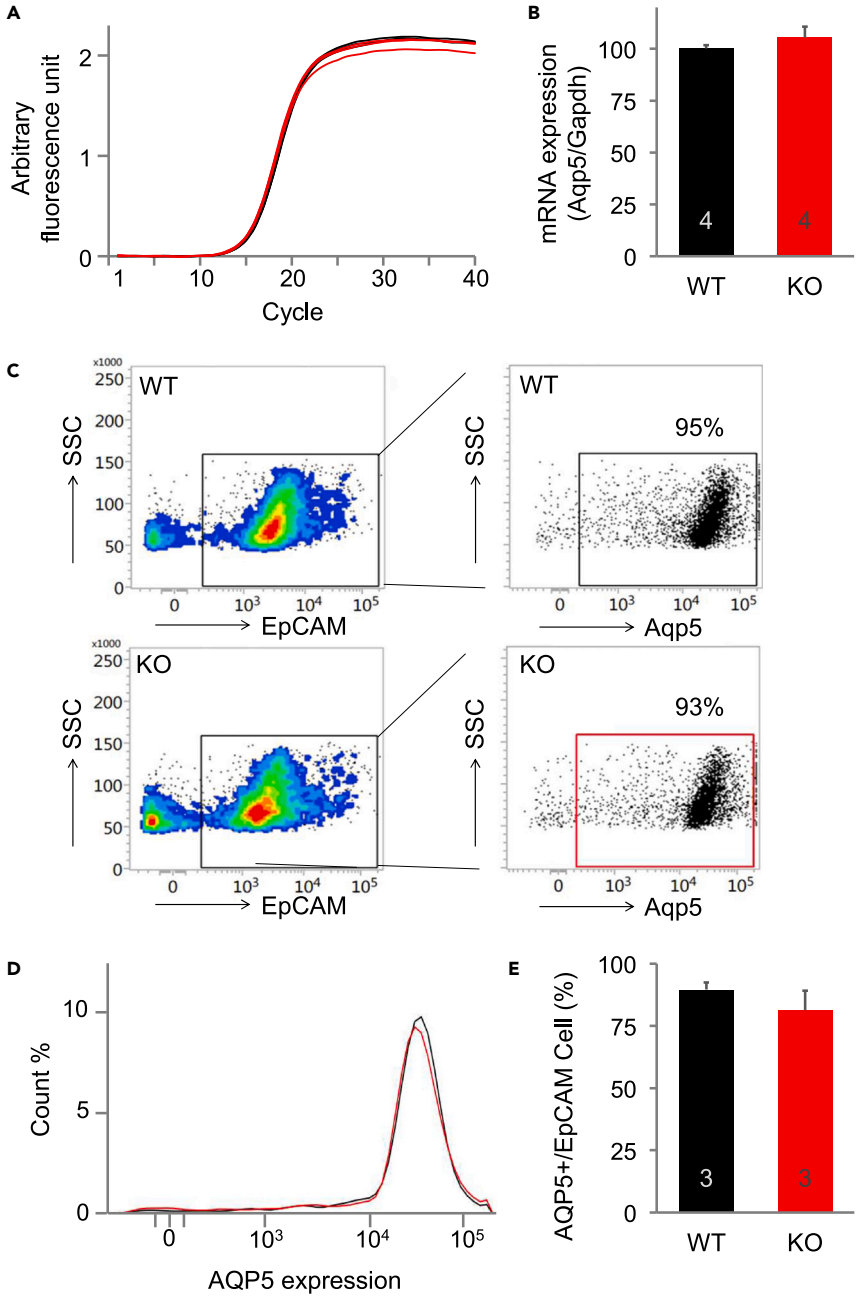

Figure 4. Expression levels of AQP5 in submandibular gland tissue of WT and *Negr1* KO mice

(A and B) Quantitative PCR analysis of AQP5 mRNA in submandibular gland cells from WT and *Negr1* KO mice.

(A) Real-time change in fluorescence with PCR cycle number in a representative quantitative PCR experiment. The result was determined in technical triplicates and data are plotted as lines.

(B) Bar graph indicating the Aqp5 mRNA expression of WT (n = 4) and *Negr1* KO mice (n = 4) was normalized to a reference gene (Gapdh).

(C–E) AQP5 surface expression of submandibular gland cells in WT and *Negr1* KO mice was measured by flow cytometry.

(C) Representative density plots are shown: Left gating of epithelial cell adhesion molecule (EpCAM)(+) cells, right gating of AQP5(+) cells. Percentages reported in the flow plots indicate the percentage of EpCAM-labeled AQP5(+) cells in SMG isolated from WT or *Negr1*KO mice.

(D) Representative histogram of EpCAM-labeled AQP5(+) cells in SMG isolated from WT or *Negr1* KO mice. The black line from the black box of WT and red line from the red box of KO in panel C.

(E) Quantification of AQP5(+) cells of EpCAM(+) cells in WT (n = 3) and *Negr1* KO mice (n = 3) by flow cytometry. Data are represented as mean ± SD.

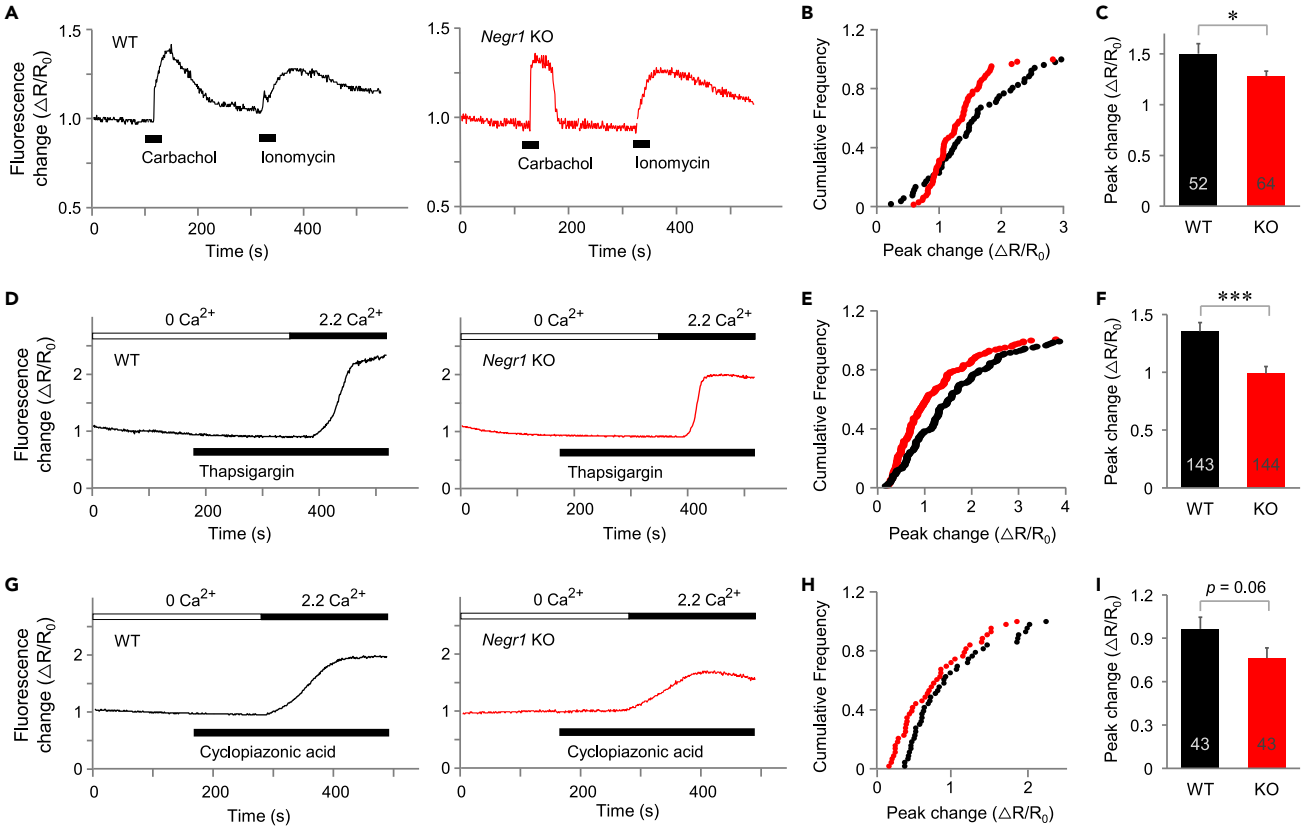

Figure 5. Impaired muscarinic Ca^{2+} signaling in *Negr1* KO mouse submandibular gland cells

(A–C) Fura-2/AM–loaded dissociated submandibular gland cells from WT (n = 52) and *Negr1* KO mice (n = 64) were treated with 100 μM of carbachol for 30 s and then with 3 μM of ionomycin for 30 s.

(A) Typical Ca^{2+} imaging traces of the fura-2 fluorescence ratio of cells.

(B) Cumulative probability of carbachol-induced Ca^{2+} increase.

(C) The quantification of carbachol-induced Ca^{2+} increase was normalized by the ionomycin-induced Ca^{2+} increase.

(D and E) Fura-2/AM–loaded dissociated submandibular gland cells from WT (n = 143) and *Negr1* KO (n = 144) mice were incubated in Ca^{2+}-free Hank's Balanced Salt Solution (HBSS) solution and stimulated with 1 μM of thapsigargin and then reincubated in 2.2 mM of Ca^{2+}-containing HBSS solution to induce store-operated Ca^{2+} entry (SOCE).

(D) Typical Ca^{2+} imaging traces showing the fura-2 fluorescence ratio of cells.

(E) Cumulative probability of the thapsigargin-induced Ca^{2+} increase.

(F) Quantification of the peak increase of the thapsigargin-mediated Ca^{2+} increase in Ca^{2+}-containing HBSS solution.

(G–I) Fura-2/AM–loaded dissociated submandibular gland cells from WT (n = 43) and *Negr1* KO (n = 43) mice were incubated in Ca^{2+}-free HBSS solution, stimulated with 10 μM of cyclopiazonic acid, and then re-incubated in 2.2 mM of Ca^{2+}-containing HBSS solution to induce SOCE.

(G) Typical Ca^{2+} imaging traces showing the fura-2 fluorescence ratio of cells.

(H) Cumulative probability of the cyclopiazonic acid-induced Ca^{2+} increase.

(I) Quantification of the peak increase of the cyclopiazonic acid-mediated Ca^{2+} increase in Ca^{2+}-containing HBSS solution. Data are represented as mean ± SEM. *p < 0.05; ***p < 0.001.

store-operated Ca^{2+} entry (SOCE) when pool depletion occurs.[2] We found that the carbachol-induced Ca^{2+} increase was decreased in *Negr1* KO mice. The intracellular Ca^{2+} increase evoked by thapsigargin (an SOCE-inducing SERCA inhibitor) was reduced as well in *Negr1* KO mice (Figures 5D–5F). In addition, we observed that cyclopiazonic acid induced Ca^{2+} influx was slightly decreased in KO mice. Because cyclopiazoic acid inhibits SERCA, this result confirms again the decrease in the store-operated Ca^{2+} entry in *Negr1* KO mice (Figures 5G–5I). We confirmed the existence of a decrease in SOCE in *Negr1* KO mice by measuring the SOCE current by whole-cell recording (Figures 6A–6C). These results indicated that NEGR1 regulates muscarinic Ca^{2+} signaling.

Next, we investigated the effects of NEGR1 on the activity of the Ca^{2+}-activated ion channels modulating the paracellular water movement. ANO1 channels are Ca^{2+}-activated Cl^- channels that are expressed in

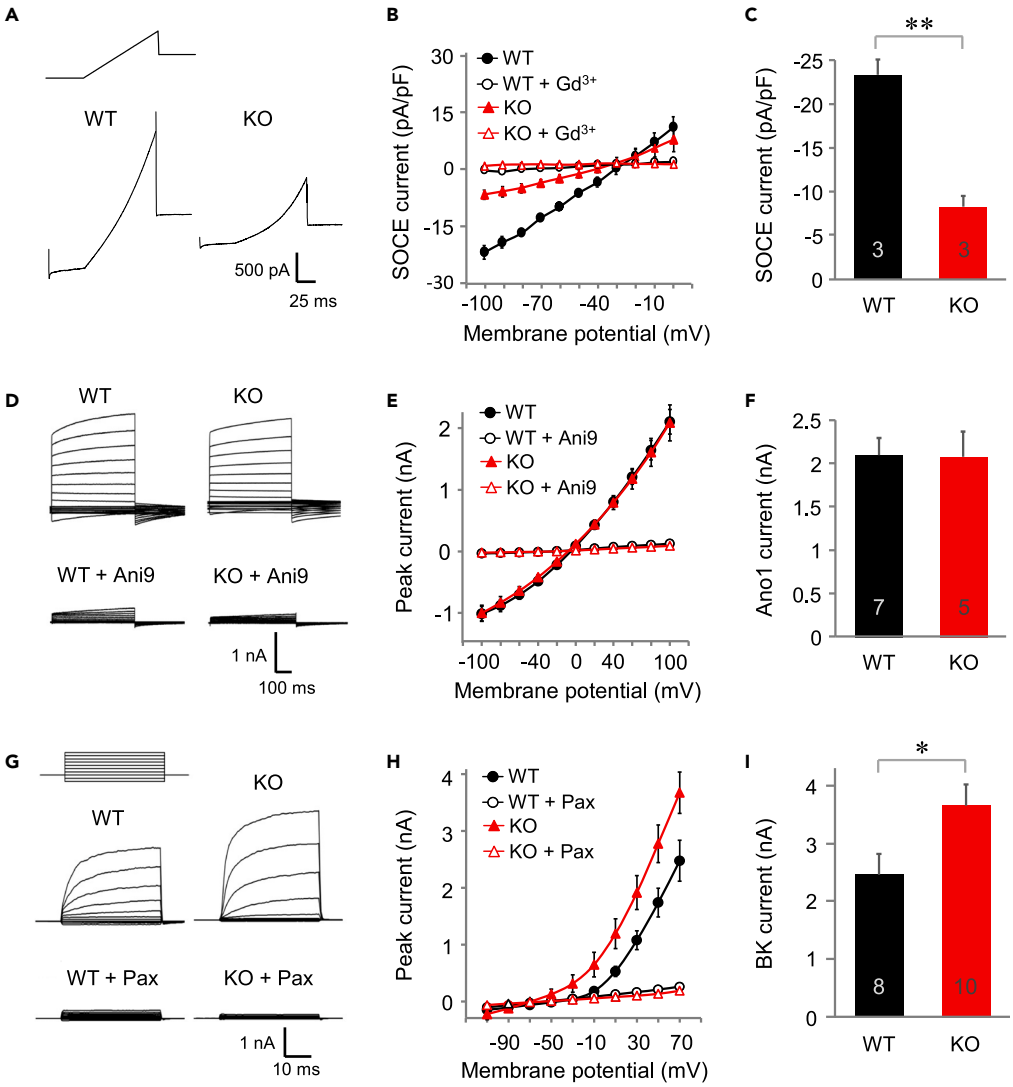

Figure 6. Decreased store-operated Ca^{2+} entry and increased large-conductance Ca^{2+}-activated K^+ channel (BK channel) activity in *Negr1* KO mice

(A) Representative current traces of SOCE currents obtained with 1 μM of thapsigargin in WT (n = 3) and *Negr1* KO mice (n = 3) submandibular gland cells. The protocol started with a 50-ms voltage step at −100 mV, then the holding voltage was linearly increased to +100 mV in 100 ms, and the last 50 ms of the protocol consisted of a voltage step of 0 mV.

(B) I–V curves of currents induced by the depletion of Ca^{2+} store with 1 μM of thapsigargin with or without the treatment with Gd^{3+} as a SOCE inhibitor.

(C) SOCE current intensity at −100 mV.

(D) Representative current traces of Ca^{2+}-activated Cl^- channel ANO1 channels in WT (n = 7) and *Negr1* KO mice (n = 5) submandibular gland cells. The cells were held at −60 mV, and depolarizing pulses from −100 to +100 mV were delivered in 20-mV increments.

(E) The I−V relationship from the peak current of the ANO1 channel with or without treatment with Ani9, a specific ANO1 inhibitor.

(F) ANO1 channel peak current at +100 mV.

(G) Representative current traces of BK channels in WT (n = 8) and *Negr1* KO mice (n = 10) submandibular gland cells. The currents were obtained by step pulses (voltage interval: 20 mV; duration: 40 ms) from −110 mV to +70 mV.

(H) The I−V curves from the peak current of the BK channel with or without treatment with paxilline (Pax), a specific BK channel inhibitor.

(I) BK channel peak current at +70 mV. Data are represented as mean ± SEM. *p < 0.05; **p < 0.01.

salivary acinar cells to generate Cl^- flow, which is a driving force for primary fluid secretion.[24] BK channels are Ca^{2+}-activated K^+ channels, which induce hyperpolarization of the acinar cell membrane and support Cl^- flow.[25] We compared ANO1 activity, and there was no difference between the two types of mice (Figures 6D–6F). Meanwhile, BK channel activity was significantly increased in *Negr1* KO mice (Figures 6G–6I).

Reduced salivary secretion in *Negr1* KO mice

Finally, we monitored the salivation in *Negr1* KO mice. We found that the salivation induced by pilocarpine (Figures 7A and 7B) and carbachol (Figure 7C) was significantly decreased in *Negr1* KO mice relative to that in WT mice. In addition, *Negr1* KO mice exhibited a decrease in the pilocarpine-induced salivary secretion specific to the submandibular gland (Figure 7D). *Negr1* +/− heterozygous female mice showed marginal decreased in salivation (Figures S1A and S1B). On the other hand, no significant difference was observed in salivation with forskolin treatment (Figure S1C). With these results, we could confirm once again that salivation was decreased in *Negr1* KO mice and that the cause was impaired muscarinic Ca^{2+} signaling.

DISCUSSION

In this article, we found that NEGR1, which is known to regulate glutamatergic neurotransmission in hippocampal dentate gyrus granular cells, is expressed in mouse salivary glands and controls salivation by regulating muscarinic transcellular water movement. Our data indicate that (1) NEGR1 is expressed in mouse and human submandibular glands; (2) *Negr1* KO mice showed decreased muscarinic Ca^{2+} signaling, especially SOCE; and (3) *Negr1* KO mice experienced impaired salivation without histological changes in the submandibular glands. With these findings, we have indicated a modulatory role of NEGR1 in salivary Ca^{2+} signaling, which contributes to salivary secretion.

In our previous report, we studied the neuronal function of NEGR1 and found that *Negr1* KO mice showed a decrease in long-term potentiation formation and an impairment of synaptogenesis.[20] In this study, we would like to emphasize the significant contribution of NEGR1 in neuro-salivary gland communication. Most of all, it is surprising that NEGR1, which is expressed at a low level, functions as an important secretion regulator. In general, it is reasonable to assume that adhesion molecules with a high molecule abundance will have a high functional significance. As the characteristics of various CAMs are revealed, it is apparent that the correlation between expression level and function is not constant. For instance, it is evident that cell adhesion molecules have functions common to most of neurons, however, the degree of expression varies considerably according to the type of neuron. Even if there is only a small amount of expression of NEGR1, it is capable of interacting with other membrane proteins such as receptors and channels[26] of which interaction will reveal its function. Therefore, identifying and characterization of NEGR1-binding partners in the future will enable more interesting studies of salivary gland function to be conducted. Another interesting issue is that the regulation of SOCE by NEGR1 was discovered in this study. It is not yet known how NEGR1 affects GPCR-mediated Ca^{2+} signaling. We assume that NEGR1 possibly affects the G protein or Orai1 channels in the plasma membrane. Further research is needed on why the loss of function of NEGR1 leads to the impairment of SOCE-mediated Ca^{2+} signaling. It would be also intriguing to examine whether NEGR1 modulates the signaling of other GPCR-PLC-linked receptors expressed in the salivary glands. In addition, it would be important to examine whether NEGR1 regulates Ca^{2+} signaling in other organs (e.g., adipocytes) where GPCRs are responsible for physiological functions, thereby regulating the function of the organ in question.

Not only salivary gland cells but also neurons contribute to salivation; as such, the decrease in salivation in *Negr1* KO mice needs to be evaluated in terms of both salivary gland cells and neurons. Previously, we found that the neurotransmitter release efficiency of the excitatory synapse was not altered in *Negr1* KO mice.[20] Therefore, the possibility that salivary dysfunction is because of changes in neurotransmitter secretion efficiency is low. However, a decrease in miniature EPSC frequency was observed in *Negr1* KO mice, indicating impaired synaptogenesis.[20] Thus, it would be interesting to elucidate whether NEGR1 regulates synaptogenesis in the salivary glands. The salivary glands secrete neurotrophin, which promotes the survival and differentiation of innervating neurons and induces synaptogenesis.[27–29] Therefore, it remains possible that the salivary dysfunction observed in *Negr1* KO mice is due in part to the impairment of the synaptogenesis that connects salivary gland cells and neurons, which is not yet understood in detail. Therefore, it would be interesting to explore these areas further using *Negr1*-conditional KO mice in the future.

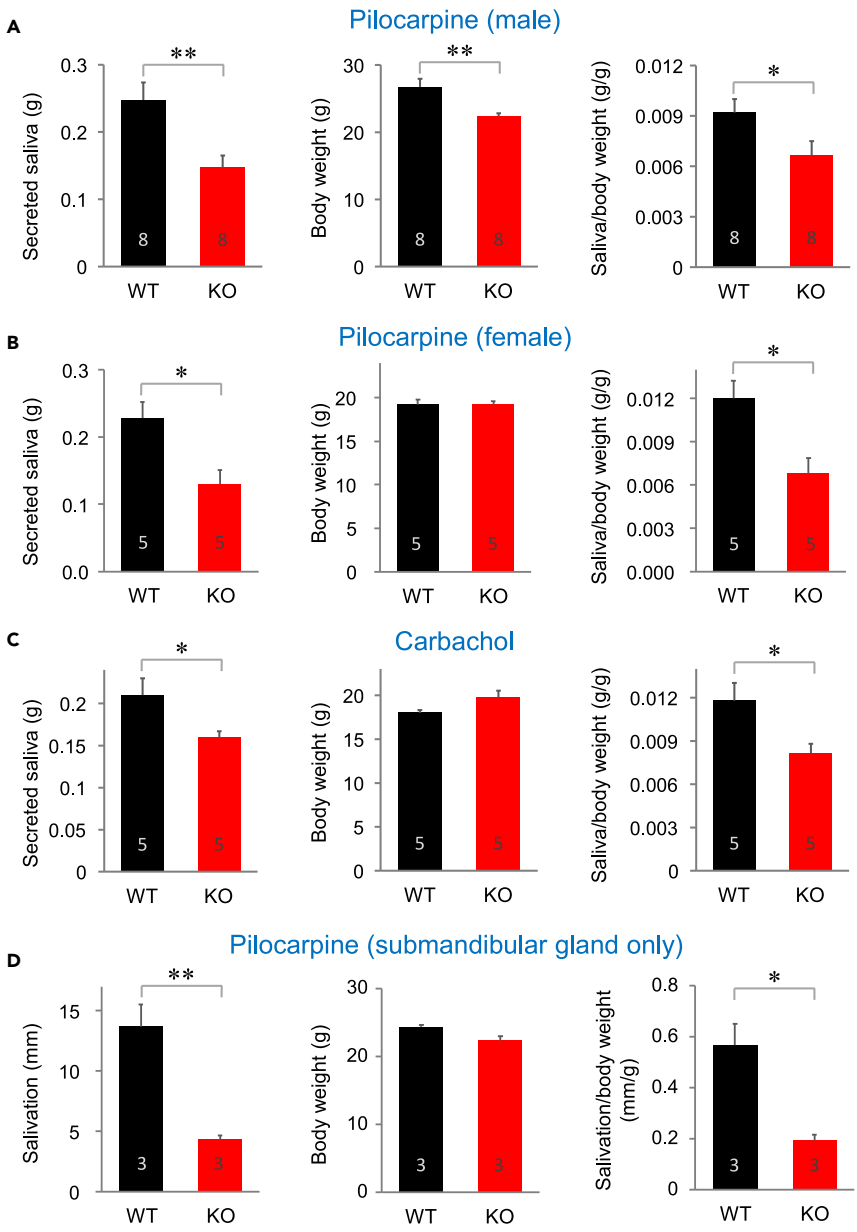

Figure 7. Pilocarpine and carbachol-mediated salivation were decreased in *Negr1* KO mice

The mice were injected with (A) 300 μg/kg pilocarpine (male WT mice, n = 8; male *Negr1* KO mice, n = 8), (B) 300 μg/kg pilocarpine (female WT mice, n = 5; female *Negr1* KO mice, n = 5), or (C) 7.4 μg/kg carbachol (male WT mice, n = 5; male *Negr1* KO mice, n = 5) and then saliva production from whole salivary glands was measured.

(D) The mice were injected with 300 μg/kg pilocarpine (male WT mice, n = 8; male *Negr1* KO mice, n = 8) and then saliva production from the submandibular glands was measured. Data are represented as salivation volume (*left*), mouse body weight (*middle*), and salivation per mouse body weight (*right*). Data are represented as means ± SEM. *p < 0.05; **p < 0.01.

It is interesting that NEGR1, which is abundant in the duct, has an impact on the amount of saliva secreted. It has long been accepted that the acinar is responsible for determining the amount of salivary secretion, whereas the duct is responsible for determining the final composition of saliva. In addition, we are certain that acinar plays a vital role in water production. However, the amount of saliva secreted has been reported to be altered by ductal changes in several studies. It was observed that hyposalivation occurred in the animal with increased expression of the salivary gland ductal SGLT1,[30,31] and in the KK-AY type-2 diabetes mellitus model which specifically altered duct function.[32] Unlike normal conditions, pathological conditions

(i.e. diabetes mellitus) show the possibility that the duct affects the salivary secretion directly or indirectly. We speculate that the loss of NEGR1, a cell adhesion molecule, may result in a dysfunctional tight junction or a mislocalization of membrane proteins in the ductal cell. A clear mechanism, however, requires further investigation. It is hoped that future studies of duct-specific factors (such as NEGR1) that affect salivary secretion will provide more clarity regarding the ductal role in salivation.

Dry mouth is caused by multiple factors, including Sjogren's syndrome. It is interesting to note that (1) leukemia inhibitory factor receptor (LIFR) which interacts with NEGR1,[33,34] and (2) lipocalin-2 of which expression is controlled by NEGR1-LIFR interaction,[35,36] play a role in regulating autoimmunity. Furthermore, the saliva and tears of patients with primary Sjogren's syndrome were found to contain increased levels of neutrophil gelatinase-associated lipocalin (NGAL), a human analogue of lipocalin-2.[37,38] Therefore, if the loss of function of NEGR1 contributes to reduced salivation, it would be interesting to examine the correlation between NEGR1 and Sjogren's syndrome. However, the bioinformatics analysis of the publicly available RNA-seq databases of Sjogren syndrome patients did not reveal any changes in NEGR1 (Figure 3), and no histological changes (such as immune cell infiltration) were observed in the submandibular gland of *Negr1* KO mice (Figure 2). Apart from Sjogren's syndrome, salivary gland hypofunction can be caused by a variety of factors. The results of our study indicate that NEGR1 alters the communication between salivary glands and nerves, specifically muscarinic Ca^{2+} signals. Recently *Negr1* gene disruption because of 1p31.1 microdeletion has been reported in two human patients; A 14-year-old female patient displayed phenotypes of intellectual disability, language delay, and disruptive behavior disorder, and a 5-month-old infant showed symptoms of global hypotonia and difficulty sucking.[39] However, to date, no NEGR1 mutation has been found in patients with dry mouth. It remains unclear whether (or how much) dry mouth occurs in patients with major depression with a *Negr1*mutation. Dry mouth has been observed in a variety of neurological and psychiatric patients, including those with anxiety,[40,41] depression,[41] schizophrenia,[42] and bipolar disorder.[42] The causal factors of dry mouth observed in neurological and psychiatric patients can be complicated by side effects from treatment drugs.[43,44] Nevertheless, it is crucial to identify the cause of dry mouth—whether genetic or drug-induced—to establish a diagnostic and treatment strategy. Study of the neuro-exocrine common factor that regulates receptor signaling will ultimately contribute to elucidating the causative mechanism of dry mouth with an unclear etiology.

Limitations of the study

We mentioned that lack of results from using Negr1-conditional KO mice as weakness of our study. In addition, we were unable to provide the experimental evidence for the NEGR1's localization to determine which cells in mouse salivary glands express NEGR1. Despite long experimental attempts, ultimately, we were unable to determine the distribution of NEGR1 despite repeated immunohistochemistry experiments. Commercially available NEGR1 antibodies were found to show the similar pattern on WT and *Negr1* KO tissue, which rendered them unsuitable for use in histological analysis. It is a reality that many other NEGR1 studies targeting the brain and adipose tissue have not yet yielded reliable histological results.

We found that male and female mice displayed slight differences in the granular convoluted tubule structures in salivary glands, but no differences in secretion amount. In light of this, relatively little is known about the structure and function of salivary glands in relation to sexual diversity, which resulted in a very interesting discovery. The majority of previous studies of salivary gland structure and function have been conducted on male mice to rule out the possibility of showing variations in various conditions (e.g. estrous cycle). We did not observe sexual diversity in the salivation of *Negr1* KO mice, so further in-depth studies have not been conducted. However, our findings are likely to raise a number of new questions.

STAR★METHODS

Detailed methods are provided in the online version of this paper and include the following:

- KEY RESOURCES TABLE
- RESOURCE AVAILABILITY
  - Lead contact
  - Materials availability
  - Data and code availability
- EXPERIMENTAL MODEL AND SUBJECT DETAILS
  - Animals

SUPPLEMENTAL INFORMATION

Supplemental information can be found online at https://doi.org/10.1016/j.isci.2023.106773.

ACKNOWLEDGMENTS

This work was supported by the National Research Foundation of Korea (2018R1A5A2024418 to S.Y.C; 2021R1A2C2005573 to H.K.P; 2020R1A5A8017671 to S.L.).

AUTHOR CONTRIBUTIONS

J.L., S.K., K.H.K., and B.L. conducted the experiments, acquiring data, and analyzing data. Y-B.K., G.C., and W.S. analyzed data. S.J.L. and S.L. provided reagents. H-K.P. and S-Y.C. designed research studies, and drafted the manuscript. All the authors participated in discussions of the research.

DECLARATION OF INTERESTS

The authors declare no competing interests.

INCLUSION AND DIVERSITY

We support inclusive, diverse, and equitable conduct of research.

Received: September 6, 2022
Revised: February 26, 2023
Accepted: April 24, 2023
Published: April 26, 2023

REFERENCES

1. Proctor, G.B., and Carpenter, G.H. (2007). Regulation of salivary gland function by autonomic nerves. Auton. Neurosci. *133*, 3–18. https://doi.org/10.1016/j.autneu.2006.10.006.

2. Ambudkar, I.S. (2016). Calcium signalling in salivary gland physiology and dysfunction. J. Physiol. *594*, 2813–2824. https://doi.org/10.1113/JP271143.

3. Gao, X., Oei, M.S., Ovitt, C.E., Sincan, M., and Melvin, J.E. (2018). Transcriptional profiling reveals gland-specific differential expression in the three major salivary glands of the adult mouse. Physiol. Genomics *50*, 263–271. https://doi.org/10.1152/physiolgenomics.00124.2017.

4. Saitou, M., Gaylord, E.A., Xu, E., May, A.J., Neznanova, L., Nathan, S., Grawe, A., Chang, J., Ryan, W., Ruhl, S., et al. (2020). Functional specialization of human salivary glands and origins of proteins intrinsic to human saliva. Cell Rep. *33*, 108402. https://doi.org/10.1016/j.celrep.2020.108402.

5. Oyelakin, A., Song, E.A.C., Min, S., Bard, J.E., Kann, J.V., Horeth, E., Smalley, K., Kramer, J.M., Sinha, S., and Romano, R.A. (2019). Transcriptomic and single-cell analysis of the murine parotid gland. J. Dent. Res. *98*, 1539–1547. https://doi.org/10.1177/0022034519882355.

6. Gluck, C., Min, S., Oyelakin, A., Smalley, K., Sinha, S., and Romano, R.A. (2016). RNA-seq based transcriptomic map reveals new insights into mouse salivary gland development and maturation. BMC Genom. *17*, 923. https://doi.org/10.1186/s12864-016-3228-7.

7. Sekiguchi, R., Martin, D.; Genomics and Computational Biology Core, and Yamada, K.M. (2020). Single-cell RNA-seq identifies cell diversity in embryonic salivary glands. J. Dent. Res. *99*, 69–78. https://doi.org/10.1177/0022034519883888.

8. Song, E.A.C., Min, S., Oyelakin, A., Smalley, K., Bard, J.E., Liao, L., Xu, J., and Romano, R.A. (2018). Genetic and scRNA-seq analysis reveals distinct cell populations that contribute to salivary gland development and maintenance. Sci. Rep. *8*, 14043. https://doi.org/10.1038/s41598-018-32343-z.

9. Hauser, B.R., Aure, M.H., Kelly, M.C., Genomics and Computational Biology Core, Hoffman, M.P., and Chibly, A.M. (2020). Generation of a single-cell RNAseq atlas of murine salivary gland development. iScience *23*, 101838. https://doi.org/10.1016/j.isci.2020.101838.

10. Shitara, A., Malec, L., Ebrahim, S., Chen, D., Bleck, C., Hoffman, M.P., and Weigert, R. (2019). Cdc42 negatively regulates endocytosis during apical membrane maintenance in live animals. Mol. Biol. Cell *30*, 324–332. https://doi.org/10.1091/mbc.E18-10-0615.

11. Kim, H., Chun, Y., Che, L., Kim, J., Lee, S., and Lee, S. (2017). The new obesity-associated protein, neuronal growth regulator 1 (NEGR1), is implicated in Niemann-Pick disease Type C (NPC2)-mediated cholesterol trafficking. Biochem. Biophys. Res. Commun. *482*, 1367–1374. https://doi.org/10.1016/j.bbrc.2016.12.043.

12. Joo, Y., Kim, H., Lee, S., and Lee, S. (2019). Neuronal growth regulator 1-deficient mice show increased adiposity and decreased muscle mass. Int. J. Obes. *43*, 1769–1782. https://doi.org/10.1038/s41366-019-0376-2.

13. Flores-Dorantes, M.T., Díaz-López, Y.E., and Gutiérrez-Aguilar, R. (2020). Environment and gene association with obesity and their impact on neurodegenerative and neurodevelopmental diseases. Front. Neurosci. *14*, 863. https://doi.org/10.3389/fnins.2020.00863.

14. Miyata, S., Matsumoto, N., Taguchi, K., Akagi, A., Iino, T., Funatsu, N., and Maekawa, S. (2003). Biochemical and ultrastructural analyses of IgLON cell adhesion molecules, Kilon and OBCAM in the rat brain. Neuroscience *117*, 645–658. https://doi.org/10.1016/s0306-4522(02)00873-4.

15. Maccarrone, G., Ditzen, C., Yassouridis, A., Rewerts, C., Uhr, M., Uhlen, M., Holsboer, F., and Turck, C.W. (2013). Psychiatric patient stratification using biosignatures based on cerebrospinal fluid protein expression clusters. J. Psychiatr. Res. *47*, 1572–1580. https://doi.org/10.1016/j.jpsychires.2013.07.021.

16. Tamási, V., Petschner, P., Adori, C., Kirilly, E., Ando, R.D., Tothfalusi, L., Juhasz, G., and Bagdy, G. (2014). Transcriptional evidence for the role of chronic venlafaxine treatment in neurotrophic signaling and neuroplasticity including also Glutamatergic [corrected] - and insulin-mediated neuronal processes. PLoS One *9*, e113662. https://doi.org/10.1371/journal.pone.0113662.

17. Dall'Aglio, L., Lewis, C.M., and Pain, O. (2021). Delineating the genetic component of gene expression in major depression. Biol. Psychiatry *89*, 627–636. https://doi.org/10.1016/j.biopsych.2020.09.010.

18. Hashimoto, T., Yamada, M., Maekawa, S., Nakashima, T., and Miyata, S. (2008). IgLON cell adhesion molecule Kilon is a crucial modulator for synapse number in hippocampal neurons. Brain Res. *1224*, 1–11. https://doi.org/10.1016/j.brainres.2008.05.069.

19. Sanz, R., Ferraro, G.B., and Fournier, A.E. (2015). IgLON cell adhesion molecules are shed from the cell surface of cortical neurons to promote neuronal growth. J. Biol. Chem. *290*, 4330–4342. https://doi.org/10.1074/jbc.M114.628438.

20. Noh, K., Lee, H., Choi, T.Y., Joo, Y., Kim, S.J., Kim, H., Kim, J.Y., Jahng, J.W., Lee, S., Choi, S.Y., and Lee, S.J. (2019). Negr1 controls adult hippocampal neurogenesis and affective behaviors. Mol. Psychiatry *24*, 1189–1205. https://doi.org/10.1038/s41380-018-0347-3.

21. Noh, K., Park, J.C., Han, J.S., and Lee, S.J. (2020). From bound cells comes a sound mind: the role of neuronal growth regulator 1 in psychiatric disorders. Exp. Neurobiol. *29*, 1–10. https://doi.org/10.5607/en.2020.29.1.1.

22. Hillen, M.R., Pandit, A., Blokland, S.L.M., Hartgring, S.A.Y., Bekker, C.P.J., van der Heijden, E.H.M., Servaas, N.H., Rossato, M., Kruize, A.A., van Roon, J.A.G., and Radstake, T. (2019). Plasmacytoid DCs from patients with sjogren's syndrome are transcriptionally primed for enhanced pro-inflammatory cytokine production. Front. Immunol. *10*, 2096. https://doi.org/10.3389/fimmu.2019.02096.

23. Chen, X., Cheng, Q., Du, Y., Liu, L., and Wu, H. (2021). Differential long non-coding RNA expression profile and function analysis in primary Sjogren's syndrome. BMC Immunol. *22*, 47. https://doi.org/10.1186/s12865-021-00439-3.

24. Romanenko, V.G., Catalán, M.A., Brown, D.A., Putzier, I., Hartzell, H.C., Marmorstein, A.D., Gonzalez-Begne, M., Rock, J.R., Harfe, B.D., and Melvin, J.E. (2010). Tmem16A encodes the Ca2+-activated Cl- channel in mouse submandibular salivary gland acinar cells. J. Biol. Chem. *285*, 12990–13001. https://doi.org/10.1074/jbc.M109.068544.

25. Romanenko, V.G., Nakamoto, T., Srivastava, A., Begenisich, T., and Melvin, J.E. (2007). Regulation of membrane potential and fluid secretion by Ca2+-activated K+ channels in mouse submandibular glands. J. Physiol. *581*, 801–817. https://doi.org/10.1113/jphysiol.2006.127498.

26. Singh, K., Loreth, D., Pöttker, B., Hefti, K., Innos, J., Schwald, K., Hengstler, H., Menzel, L., Sommer, C.J., Radyushkin, K., et al. (2018). Neuronal growth and behavioral alterations in mice deficient for the psychiatric disease-associated Negr1 gene. Front. Mol. Neurosci. *11*, 30. https://doi.org/10.3389/fnmol.2018.00030.

27. Heuckeroth, R.O., Enomoto, H., Grider, J.R., Golden, J.P., Hanke, J.A., Jackman, A., Molliver, D.C., Bardgett, M.E., Snider, W.D., Johnson, E.M., Jr., and Milbrandt, J. (1999). Gene targeting reveals a critical role for neurturin in the development and maintenance of enteric, sensory, and parasympathetic neurons. Neuron *22*, 253–263. https://doi.org/10.1016/s0896-6273(00)81087-9.

28. Ferreira, J.N., and Hoffman, M.P. (2013). Interactions between developing nerves and salivary glands. Organogenesis *9*, 199–205. https://doi.org/10.4161/org.25224.

29. Sommakia, S., and Baker, O.J. (2016). Neurons self-organize around salivary epithelial cells in novel Co-culture model. J. Stem Cell Regen. Biol. *2*, 1–6. https://doi.org/10.15436/2471-0598.16.013.

30. Sabino-Silva, R., Freitas, H.S., Lamers, M.L., Okamoto, M.M., Santos, M.F., and Machado, U.F. (2009). Na+-glucose cotransporter SGLT1 protein in salivary glands: potential involvement in the diabetes-induced decrease in salivary flow. J. Membr. Biol. *228*, 63–69. https://doi.org/10.1007/s00232-009-9159-3.

31. Sabino-Silva, R., Okamoto, M.M., David-Silva, A., Mori, R.C., Freitas, H.S., and Machado, U.F. (2013). Increased SGLT1 expression in salivary gland ductal cells correlates with hyposalivation in diabetic and hypertensive rats. Diabetol. Metab. Syndr. *5*, 64. https://doi.org/10.1186/1758-5996-5-64.

32. Munemasa, T., Mukaibo, T., Kondo, Y., Masaki, C., Kusuda, Y., Miyagi, Y., Tsuka, S., Hosokawa, R., and Nakamoto, T. (2018). Salivary gland hypofunction in KK-A(y) type 2 diabetic mice. J. Diabetes *10*, 18–27. https://doi.org/10.1111/1753-0407.12548.

33. Linker, R.A., Kruse, N., Israel, S., Wei, T., Seubert, S., Hombach, A., Holtmann, B., Luhder, F., Ransohoff, R.M., Sendtner, M., and Gold, R. (2008). Leukemia inhibitory factor deficiency modulates the immune response and limits autoimmune demyelination: a new role for neurotrophic cytokines in neuroinflammation. J. Immunol. *180*, 2204–2213. https://doi.org/10.4049/jimmunol.180.4.2204.

34. Cao, W., Yang, Y., Wang, Z., Liu, A., Fang, L., Wu, F., Hong, J., Shi, Y., Leung, S., Dong, C., and Zhang, J.Z. (2011). Leukemia inhibitory factor inhibits T helper 17 cell differentiation and confers treatment effects of neural progenitor cell therapy in autoimmune disease. Immunity *35*, 273–284. https://doi.org/10.1016/j.immuni.2011.06.011.

35. Berard, J.L., Zarruk, J.G., Arbour, N., Prat, A., Yong, V.W., Jacques, F.H., Akira, S., and David, S. (2012). Lipocalin 2 is a novel immune mediator of experimental autoimmune encephalomyelitis pathogenesis and is modulated in multiple sclerosis. Glia *60*, 1145–1159. https://doi.org/10.1002/glia.22342.

36. Nam, Y., Kim, J.H., Seo, M., Kim, J.H., Jin, M., Jeon, S., Seo, J.W., Lee, W.H., Bing, S.J., Jee, Y., et al. (2014). Lipocalin-2 protein deficiency ameliorates experimental autoimmune encephalomyelitis: the pathogenic role of lipocalin-2 in the central nervous system and peripheral lymphoid tissues. J. Biol. Chem. *289*, 16773–16789. https://doi.org/10.1074/jbc.M113.542282.

37. Aqrawi, L.A., Galtung, H.K., Guerreiro, E.M., Øvstebø, R., Thiede, B., Utheim, T.P., Chen, X., Utheim, Ø.A., Palm, Ø., Skarstein, K., and Jensen, J.L. (2019). Proteomic and histopathological characterisation of sicca subjects and primary Sjogren's syndrome patients reveals promising tear, saliva and extracellular vesicle disease biomarkers. Arthritis Res. Ther. *21*, 181. https://doi.org/10.1186/s13075-019-1961-4.

38. Aqrawi, L.A., Jensen, J.L., Fromreide, S., Galtung, H.K., and Skarstein, K. (2020). Expression of NGAL-specific cells and mRNA levels correlate with inflammation in the salivary gland, and its overexpression in the saliva, of patients with primary Sjogren's syndrome. Autoimmunity *53*, 333–343. https://doi.org/10.1080/08916934.2020.1795140.

39. Tassano, E., Uccella, S., Giacomini, T., Fiorio, P., Tavella, E., Malacarne, M., Gimelli, G., Coviello, D., and Ronchetto, P. (2020). 1p31.1 microdeletion including only NEGR1 gene in two patients. Eur. J. Med. Genet. *63*, 103919. https://doi.org/10.1016/j.ejmg.2020.103919.

40. Veerabhadrappa, S.K., Chandrappa, P.R., Patil, S., Roodmal, S.Y., Kumarswamy, A., and Chappi, M.K. (2016). Evaluation of xerostomia in different psychological disorders: an observational study. J. Clin. Diagn. Res. *10*, ZC24–ZC27. https://doi.org/10.7860/JCDR/2016/19020.8437.

41. Gholami, N., Hosseini Sabzvari, B., Razzaghi, A., and Salah, S. (2017). Effect of stress, anxiety and depression on unstimulated salivary flow rate and xerostomia. J. Dent. Res. Dent. Clin. Dent. Prospects *11*, 247–252. https://doi.org/10.15171/joddd.2017.043.

42. Helfer, B., Samara, M.T., Huhn, M., Klupp, E., Leucht, C., Zhu, Y., Engel, R.R., and Leucht, S. (2016). Efficacy and safety of antidepressants added to antipsychotics for schizophrenia: a systematic review and meta-analysis. Am. J. Psychiatry *173*, 876–886. https://doi.org/10.1176/appi.ajp.2016.15081035.

43. Cappetta, K., Beyer, C., Johnson, J.A., and Bloch, M.H. (2018). Meta-analysis: risk of dry mouth with second generation antidepressants. Prog. Neuropsychopharmacol. Biol. Psychiatry *84*, 282–293. https://doi.org/10.1016/j.pnpbp.2017.12.012.

44. Bessonova, L., Velligan, D.I., Weiden, P.J., O'Sullivan, A.K., Yarlas, A., Bayliss, M., Baranwal, N., Rychlec, K., Carpenter-Conlin, J., Doane, M.J., and Sajatovic, M. (2020). Antipsychotic treatment experiences of people with bipolar I disorder: patient perspectives from an online survey. BMC Psychiatry *20*, 354. https://doi.org/10.1186/s12888-020-02767-x.

45. Horeth, E., Oyelakin, A., Song, E.A.C., Che, M., Bard, J., Min, S., Kiripolsky, J., Kramer, J.M., Sinha, S., and Romano, R.A. (2021). Transcriptomic and single-cell analysis reveals regulatory networks and cellular heterogeneity in mouse primary sjogren's syndrome salivary glands. Front. Immunol. *12*, 729040. https://doi.org/10.3389/fimmu.2021.729040.

46. Lee, J., Kim, S., Kim, H.M., Kim, H.J., and Yu, F.H. (2019). NaV1.6 and NaV1.7 channels are major endogenous voltage-gated sodium channels in ND7/23 cells. PLoS One *14*, e0221156. https://doi.org/10.1371/journal.pone.0221156.

47. Park, Y.H., Son, C., Seo, Y.M., Lee, Y.S., Har, A., and Park, J.C. (2021). CPNE7-Induced autophagy restores the physiological function of mature odontoblasts. Front. Cell Dev. Biol. *9*, 655498. https://doi.org/10.3389/fcell.2021.655498.

48. Wu, X., Amorn, M.M., Aujla, P.K., Rice, S., Mimms, R., Watson, A.M., Peters-Hall, J.R., Rose, M.C., and Peña, M.T. (2011). Histologic characteristics and mucin immunohistochemistry of cystic fibrosis sinus mucosa. Arch. Otolaryngol. Head Neck Surg. *137*, 383–389. https://doi.org/10.1001/archoto.2011.34.

49. Bagavant, H., Trzeciak, M., Papinska, J., Biswas, I., Dunkleberger, M.L., Sosnowska, A., and Deshmukh, U.S. (2018). A method for the measurement of salivary gland function in mice. J. Vis. Exp. https://doi.org/10.3791/57203.

50. Musheer Aalam, S.M., Viringipurampeer, I.A., Walb, M.C., Tryggestad, E.J., Emperumal, C.P., Song, J., Xu, X., Saini, R., Lombaert, I.M.A., Sarkaria, J.N., et al. (2022). Characterization of transgenic NSG-SGM3 mouse model of precision radiation-induced chronic hyposalivation. Radiat. Res. *198*, 243–254. https://doi.org/10.1667/RADE-21-00237.1.

51. Lee, J., Kim, Y.J., Choi, L.M., Lee, K., Park, H.K., and Choi, S.Y. (2021). Muscarinic receptors and BK channels are affected by lipid raft disruption of salivary gland cells. Int. J. Mol. Sci. *22*, 4780. https://doi.org/10.3390/ijms22094780.

52. Seo, J., Koo, N.Y., Choi, W.Y., Kang, J.A., Min, J.H., Jo, S.H., Lee, S.J., Oh, S.B., Kim, J.S., Lee, J.H., et al. (2010). Sphingosine-1-phosphate signaling in human submandibular cells. J. Dent. Res. *89*, 1148–1153. https://doi.org/10.1177/0022034510376044.

53. Jung, J., Nam, J.H., Park, H.W., Oh, U., Yoon, J.H., and Lee, M.G. (2013). Dynamic modulation of ANO1/TMEM16A HCO3(-) permeability by Ca2+/calmodulin. Proc. Natl. Acad. Sci. USA *110*, 360–365. https://doi.org/10.1073/pnas.1211594110.

54. Sukumaran, P., Sun, Y., Zangbede, F.Q., da Conceicao, V.N., Mishra, B., and Singh, B.B. (2019). TRPC1 expression and function inhibit ER stress and cell death in salivary gland cells. FASEB Bioadv. *1*, 40–50. https://doi.org/10.1096/fba.1021.

55. Goecks, J., Nekrutenko, A., and Taylor, J.; Galaxy Team (2010). Galaxy: a comprehensive approach for supporting accessible, reproducible, and transparent computational research in the life sciences. Genome Biol. *11*, R86. https://doi.org/10.1186/gb-2010-11-8-r86.

STAR★METHODS

KEY RESOURCES TABLE

REAGENT or RESOURCE	SOURCE	IDENTIFIER
Antibodies		
Goat-anti E-cadherin	R&D Systems	Cat# AF-748; RRID:AB_355568
Mouse-anti AQP5	Santa Cruz Biotechnology	Cat# sc-514022; RRID:AB_2891066
HRP-conjugated goat-anti mouse	Jackson ImmunoResearch	Cat# 115-035-003; RRID: AB_10015289
HRP-conjugated donkey-antigoat	Jackson ImmunoResearch	Cat# 705-035-147; RRID: AB_2313587
Goat polyclonal anti-AQP5	Santa Cruz Biotechnology	Cat# sc-9891; RRID:AB_2059874
Mouse monoclonal anti-E Cadherin	BD Biosciences	Cat# 610181; RRID:AB_397580
Alexa Fluor 647-conjugated donkey anti-goat IgG	Invitrogen	Cat# A-21447; RRID:AB_2535864
Alexa Fluor 488-conjugated donkey anti-mouse IgG	Invitrogen	Cat# A-21202; RRID:AB_141607
Alexa Fluor 647-conjugated rabbit anti-AQP5	Abcam	Cat# ab215225
PE-conjugated rat anti-EpCAM	Thermo Fisher Scientific	Cat#12-5791-82; RRID:AB_953615
Chemicals, peptides, and recombinant proteins		
Superscript III	Invitrogen	Cat# 18080-093
Solg™ 2X Taq PCR Smart mix 2	SolGent	Cat# STD02-M50h
Xylene	Duksan Chemicals	Cat# UN1307
Hematoxylin	Vector Laboratories	Cat# H-3401
Eosin	T & I	Cat# BEY-9005
Trypsin–EDTA	Gibco Laboratories	Cat# 25200-056
Collagenase	Sigma-Aldrich	Cat# C6885
Dulbecco's modified eagle medium	Gibco Laboratories	Cat#10569-010
Fura-2/AM	Invitrogen	Cat# F1201
Pluronic F-127	Molecular Probes	Cat# P3000MP
SYBR Premix Ex Taq	Takara	Cat# RR420A
Experimental models: Organisms/strains		
Mouse: C57BL6	Orientbio	N/A
Mouse: Negr1$^{-/-}$	Dr. Sung Joong Lee	N/A
Deposited data		
scRNAseq (GSE1274697)	Sekiguchi et al.[7]	GEO:GSE1274697
scRNAseq (GSE17564954)	Horeth et al.[45]	GEO:GSE17564954
RNAseq(GSE135635)	Joo et al.[12]	GEO:GSE135635
RNAseq(GSE164885)	Flores-Dorantes et al.[13]	GEO:GSE164885
Oligonucleotides		
Mouse *Negr1* (for PCR)	Noh et al.[20]	N/A
Mouse *Gapdh* (for PCR)	Lee et al.[46]	N/A
Human *Negr1* (for PCR)	This paper	N/A
Human *Gapdh* (for PCR)	This paper	N/A

(*Continued on next page*)

Continued

REAGENT or RESOURCE	SOURCE	IDENTIFIER
Mouse AQP5 (for single cell RT-PCR)	This paper	N/A
Software and algorithms		
Zen3.5	Zeiss	https://www.zeiss.com/microscopy/int/products/microscope-software/zen.html
Metafluor 6	Molecular Devices	https://www.moleculardevices.com
PATCHMASTER	HEKA Elektronik	https://heka.com
FACSUITE	BD Biosciences	https://www.bdbiosciences.com
QuantStudio™ real-time PCR detection system	Applied Biosystems	https://www.thermofisher.com/qpcr
BioRender	BioRender	https://www.biorender.com

RESOURCE AVAILABILITY

Lead contact

Further information and requests for resources and reagents should be directed to the lead contact and corresponding author, Se-Young Choi (sychoi@snu.ac.kr).

Materials availability

All unique/stable reagents generated in this study are available from the corresponding author with a completed Materials Transfer Agreement.

Data and code availability

All data reported in this paper will be shared by the lead contact upon request.

No original code was reported in this study.

Any additional information required to reanalyse the data reported in this paper is available from the lead contact upon request.

EXPERIMENTAL MODEL AND SUBJECT DETAILS

Animals

All male and female mice were housed in an animal facility with a specific pathogen-free barrier under in a controlled environment at 22–24°C, 55% humidity and a 12-h light/dark cycle. Mice were allowed access to food and water *ad libitum*. All experiments were performed on wild-type (C57BL/6N) and *Negr1* KO mice of C57BL/6N background with the experimental procedures to reduce pain, suffering and distress. The mice were allowed unlimited access to standard chow and water prior to the experiments. In addition, they were deprived of food and water for at least two hours before the experiment. Typically, experiments begin at 2 pm and last for two to three hours. It took 30 minutes to extract the salivary glands from a mouse. The mice were anesthetized with a mixture of xylene and ketamine and sacrificed by decapitation for measuring weigh of the gland. Histological studies were conducted on the male and female mice after they had been fixed by cardiac perfusion. We followed the Animal Research: Reporting *In Vivo* Experiments (ARRIVE) guidelines 2.0. All procedures were conducted in accordance with the Guide for the Care and Use of Laboratory Animals and were approved by the Seoul National University Institutional Animal Care and Use Committee (SNU IACUC).

METHOD DETAILS

RNA isolation and PCR

Total RNA was prepared from the cerebral cortex, hippocampus, stomach, and submandibular glands of C57BL/6 mice and submandibular glands of *Negr1* KO mice. The tissues were homogenized in Trizol reagent (Ambion, Austin, TX, USA), and RNA was extracted according to the manufacturer's protocol. Complementary DNA (cDNA) was reverse-transcribed from 2 μg total RNA primed with 10-pmole oligo-dT in a 20-μl reaction containing SuperScript™ III reverse transcriptase (18080093; Thermo Fischer Scientific,

Waltham, MA, USA). PCR analysis was performed using Solg™ 2X Taq PCR Smart mix 2 (STD02-M50h; SolGent, Daejeon, Republic of Korea), 1 μl cDNA template from the reverse transcription reaction, and forward and reverse primers (each 0.8 mM) in a 20-μl reaction. The protocol consisted of incubation at 95°C for 2 minutes, followed by 35 cycles of 95°C for 20 seconds, 55°C for 40 seconds, and 72°C for 20 seconds, which was then extended at 72°C for 5 minutes in a SimpliAmp thermocycler (Applied Biosystems, Waltham, MA, USA). All of the amplified reaction product was electrophoresed on a 1.5% agarose gel. Mouse *Negr1*-specific PCR primers were designed as follows: 5′-gcttctgagcctgtgctctt-3′ (forward) and 5′-cacttgtcacctccagcaaa-3′ (reverse). Human *Negr1*-specific PCR primers were designed as follows: 5′-cagcctgtgctgcctgcta-3′ (forward) and 5′-cacttatcacctcccgcaaa-3′ (reverse). PCR primers for *Gadph* were designed as follows: 5′-gtcttcaccaccatggaga-3′(forward) and 5′-aagcagttggtggtgcag-3′ (reverse).

Hematoxylin and eosin staining

Hematoxylin and eosin staining was performed according to a previously published method.[47] SMG samples were fixed in 4% paraformaldehyde overnight at 4°C and embedded in paraffin. Tissue sections (5 μm) were deparaffinized in xylene (UN1307; Duksan Chemicals, Ansan, Republic of Korea) and rehydrated with ethanol. The samples were stained with hematoxylin (H-3401; Vector Laboratories, Burlingame, CA, USA) for 4 minutes and eosin (BEY-9005; T & I, Chuncheon, Republic of Korea) for 2 minutes. Images from the sections were captured by a digital upright fluorescence microscope (Olympus BX51; Olympus Corporation, Tokyo, Japan).

Tissue protein purification

Following cardiac perfusing *Negr1*$^{-/-}$ and WT mice (8-week-old) with 0.1 M phosphate-buffered saline, we isolated submandibular salivary glands, then immediately put them into the RIPA lysis buffer with 1✕ protease inhibitor (Sigma-Aldrich, Saint Louis, MO, USA) and phosphatase inhibitor (1 mM Na_3VO_4, 1 mM NaF). On the same day of salivary gland isolation, we extracted its proteins and determined the total protein concentrations using a BCA protein assay kit (Thermo Scientific, Waltham, MA, USA, 23227). We aliquoted proteins (0.5 μg/ml) with SDS-PAGE sample buffer and denatured them at 95°C for 5 min.

SDS-PAGE

To broaden the gaps between the target and its surrounding bands, we used 8% and 12% running gels for E-cadherin and AQP5, respectively. Tris-glycine SDS running buffer (25 mM Tris, 192 mM glycine, 0.1% SDS) was used for electrophoresis. After electrophoresis, we transferred proteins onto the nitrocellulose membranes with 20% methanol-contained tris-glycine SDS transfer buffer (48 mM, 39 mM, 0.037% SDS) at 100 mV for 2 h.

Western blotting

We blocked blotted membranes with blocking buffer (5% bovine serum albumin (BSA) in Tris-buffered saline with 0.05% tween-20 (TBST)) for 1 hat room temperature, then incubated with primary antibodies (goat-anti E-cadherin, AF-748, R&D Systems, Minneapolis, MN, USA, 1:2000, mouse-anti AQP5, sc-514022, Santa Cruz Biotechnology, Delaware Avenue Santa Cruz, CA, USA, 1:2000, mouse-anti β-actin, A2228, Sigma-Aldrich, 1:2000) for 16–21 hat 4 C. After washing with TBST 10 min three times, and we incubated the membranes with HRP-conjugated secondary antibodies (goat-anti mouse, 115-035-141, 1:1000; donkey-anti-goat, 705-035-147, 1:1000, Jackson ImmunoResearch, West Grove, PA, USA) for 1.5 hat room temperature. The immunoblotting was visualized using the enhanced chemiluminescence reagent (ECL; AbFrontier, LF-QC0103, Seoul, South Korea). When we used the membranes more than once, we removed antibodies with a low-pH stripping buffer (pH 2.2; 200 mM glycine, 1% SDS, 0.03% Tween-20) for 5–10 minat RT and then re-start the blocking step.

Immunofluorescent staining

Immunofluorescent staining was performed according to a previously published method.[48] The deparaffinized and rehydrated tissue sections on slides were washed with 0.15% Triton X-100 in PBS (PBST). The endogenous peroxidase activity was blocked using 0.6% hydrogen peroxide in methyl alcohol for 20 min. Following washing with PBST, nonspecific binding sites were blocked for 60 min with 3% BSA. The slides were then incubated overnight at 4°C with the appropriate primary antibody. After being washed with PBST, the slides were incubated for 2 hr at room temperature with the appropriate secondary antibody. The primary antibodies used were sc9891 (Santa Cruz Biotechnology, Dallas, TX,

USA) for anti-AQP5 and #610181 (BD Biosciences, San Jose, CA, USA) for anti-E-cadherin. Secondary antibodies were Alexa Fluor 647-conjugated anti-goat secondary (1:200; Invitrogen, Waltham, MA, USA) and Alexa Fluor 488-conjugated anti-rabbit secondary (1:200, Invitrogen) antibodies. Finally, the slides were covered with mounting medium that contained DAPI. After mounting, images from the sections were captured by a digital upright fluorescence microscope (Olympus BX51; Olympus Corporation, Tokyo, Japan).

Salivation measurement

Salivation from mice was measured according to a previously published method.[49] A deeply anesthetized and immobilized mouse was injected intraperitoneally with secretagogues. Next, preweighed dry swabs were immediately placed into the oral cavity for 15 minutes for collection of the secreted saliva; wet swabs were then transferred to a microfuge tube, and the difference between the wet weight and dry weight was calculated to obtain the weight of saliva produced. To measure saliva from the submandibular gland specifically, we used Schirmer tear flow test strips (501–757, Surgo Surgical Supply) as described previously.[50] After the mouse had been anesthetized with a mix of xylene and ketamine, the mouth of the immobilized animal was opened, and the tongue was fixed with silkam (P00000PB, B.Braun). A mouse was injected intraperitoneally with pilocarpine, and Schirmer strips were soaked for 10 minutes to measure saliva secreted from the submandibular glands.

Mouse submandibular gland cell preparation

Isolated mouse submandibular gland cells were prepared according to a previously published method.[51] Mouse submandibular glands were surgically removed, finely minced with scissors, and digested for 5 minutes in 0.02% trypsin–EDTA (25200-056; Gibco Laboratories, Gaithersburg, MD, USA) and 0.5 mg/ml of collagenase (C6885; Sigma-Aldrich, St. Louis, MO, USA) in serum-free Dulbecco's modified eagle medium (DMEM, 10569-010; Gibco Laboratories, Gaithersburg, MD, USA). The cells were dispersed by trituration through a heat-polished Pasteur pipette 10 times every 10 minutes using decreasing pore sizes (L-M-S). Next, the cells were centrifuged at 190 × g for one minute and then washed twice with serum-free Dulbecco's modified eagle medium. The resuspended cells in serum-free media were then filtered through a 40-μm cell strainer (Becton, Dickinson and Company, Franklin Lakes, NJ, USA). Finally, the cells were attached to poly D-lysine–coated glass coverslips or a 35-mm dish.

Ca^{2+} imaging

Ca^{2+} imaging was performed according to a previously published method.[52] Cells were isolated as described above and loaded with 2 μM fura-2/AM and 0.01% pluronic F-127 (Molecular Probes, Eugene, OR, USA) for 40 minutes at 37°C. The cells on coverslips were mounted onto the inverted microscope (Olympus IX70; Olympus Corporation) and perfused continuously at 2 ml/min by a bath solution containing (mM) 140 NaCl, 5 KCl, 1 $MgCl_2$, 2 $CaCl_2$, 10 HEPES, and 10 glucose (pH 7.20). All measurements were performed at room temperature. Cells were illuminated with a 175-W xenon arc lamp, and excitation wavelengths (340/380 nm) were selected by a Lambda DG-4 monochromator filter changer (Sutter Instrument Company, Novato, CA, USA). The intracellular free calcium concentration was measured by digital video microfluorometry with an intensified charge-coupled device camera (CasCade; Roper Scientific, Sarasota, FL, USA) coupled to a microscope and a software program (Metafluor 6; Molecular Devices, San Jose, CA, USA).

Electrophysiology

ANO1, BK, SOCE activities were measured in mouse salivary gland acinar cells using whole-cell patch-clamp techniques. For measuring ANO1 channel current,[53] the patch pipette solution was contained within a solution containing (mM) 148 N-methyl-D-glucamine-Cl (NMDG-Cl), 10 EGTA, 7.4 $CaCl_2$, 3 MgATP, and 10 HEPES (pH 7.2). The external bath solution contained (mM) 146 NMDG-Cl, 1 $CaCl_2$, 1 $MgCl_2$, 10 HEPES, and 5 glucose (pH 7.4). The stimulation protocol to generate current–voltage relationships consisted of 500-ms voltage steps from −100 to +100 mV in 20-mV increments, starting from a holding potential of −60 mV. For measuring BK channel current,[51] the patch pipette solution was contained within a solution containing (mM) 135 K-glutamate, 5 EGTA, 3 $CaCl_2$, and 10 HEPES (pH 7.2). The external bath solution contained (mM) 150 Na-glutamate, 5 K-glutamate, 2 $CaCl_2$, 2 $MgCl_2$, and 10 HEPES (pH 7.2). The stimulation protocol to generate current-voltage relationships consisted of 40-ms voltage steps from −110 to +70 mV in 20-mV increments starting from a holding potential of −70 mV. For measuring SOCE current,[54] the patch

pipette solution was contained within a solution containing (mM) 150 Cesium methane sulfonate, 8 NaCl, and 10 HEPES (pH 7.2). The external bath solution contained (mM) 145 NaCl, 5 CsCl, 1 $CaCl_2$, 1 $MgCl_2$, 10 HEPES, and 10 glucose (pH 7.3). With holding potential 0 mV, voltage ramps ranging from −100 mV to +100 mV and 100 milliseconds duration were delivered at 2 seconds intervals after whole-cell configuration was formed. Whole-cell patch-clamp recordings were obtained using a HEKA EPC-9 amplifier (HEKA Elektronik, Lambrecht, Germany). Data were acquired and analyzed using the PATCHMASTER software program (HEKA Elektronik).

Flow cytometry

To evaluate the surface AQP5 expression, we used flow cytometry performed according to a previously published method.[51] Mouse dissociated submandibular cells were obtained by mashing using a 100-μm cell strainer, followed by washing the cell strainer twice with 5 ml of 0.5% bovine serum albumin (BSA) in phosphate-buffered saline (PBS). The cells were centrifuged at 190 × g and washed twice with 0.5% BSA in PBS. The cells were washed, and blocked with 2% BSA in PBS. After blocking, the cells were washed and resuspended in 100 μL of Alexa Fluor 647–conjugated AQP5 antibody (ab215225, 1:500; Abcam) and PE-conjugated EpCAM antibody (12-5791-82, 1:200, eBioscience, San Diego, CA, USA) and incubated for 30 minutes at 4°C in the dark. All of the washing steps were carried out using 1% FBS in PBS as washing buffer, followed by centrifugation (8,000 rpm for one minute at 4°C). The labeled cells were kept on ice until analysis. The cell samples were acquired on a FACSVerse flow cytometer equipped with the FACSUITE software program (BD Biosciences, San Jose, CA, USA).

Quantitative real-time PCR

To measure quantitative *Aqp5* mRNA in submandibular glands, we used previously described methods[46] and performed using the SYBR Premix Ex Taq (RR420A; Takara, Tokyo, Japan) and the QuantStudio™ real-time PCR detection system (Applied Biosystems, Waltham, MA, USA). cDNAs were amplified in 20 μl PCR reactions using 1 μl of RT reaction. Reactions with appropriate melting curve were selected for analysis and all primer sets were analyzed in triplicate. The *Gapdh* mRNA level was used as an internal control to normalize the values for transcript abundance of *Aqp5* genes. We performed four qRT-PCR experiments and averaged from triplicate analysis of each experiment.

Single cell RNA sequence analysis

Two published scRNA-seq datasets of SMGs from embryonic day 12 (E12) (GEO: GSE127469[7]) and adult mice (GEO: GSE175649[45]) were downloaded and analyzed using the Seurat 4.1.0 R package. Cells with the total number of molecules (nCount_RNA) less than 40,000, the number of detected genes (nFeature_RNA) between 200 and 5,000, and mitochondrial transcript less than 50% were used for subsequent analysis after normalized using Seurat's logNormalize with a scale factor of 10,000. The dimensional reduction was performed by t-distributed stochastic neighbor embedding (tSNE) or Uniform Manifold Approximation and Projection (UMAP) algorithms on 2,000 highly variable genes and clustered by a shared nearest neighbor (SNN) modularity optimization-based clustering algorithm. The clusters were annotated according to an expression of known cell type-specific markers. Epithelial populations were identified by expression of Epcam (all epithelium), Cftr (striated duct), Ngf and Egf (GCT), Krt14, and Krt5 (basal duct), Gstt1 (intercalated duct), Acta2 (myoepithelial cells), and Aqp5 (acinar cells). Non-epithelial clusters were identified by expression of Col1a1 (stromal cells), Pecam1 (endothelial), Cd68 (macrophages), Icos (T cells), Kit (mast cells), Nkg7 and Gzma (NK cells), Acta2+Epcam- (smooth muscle), and Alas2+ (erythroid). Embryonic day 12 populations were identified by expression of Krt14 and Krt5 (basal duct), Krt19 (duct), Sox10 (bud), Tubb3 (neuronal), Acta2+Epcam- (smooth muscle) Col1a1 (mesenchyme), Pecam1 (endothelial), and Cd68 (macrophages).

RNA sequence analysis

Raw and processed RNA-seq datasets were deposited in the National Center for Biotechnology Information Gene Expression Omnibus, accession numbers GEO: GSE135635 and GEO: GSE164885.[22,23] RNA expression datasets and details were collected from the SRA database (SRP301904, SRP217937). Reads were processed using the genome analysis tool Galaxy.[55] The analysis starts from data uploading using FastQ. RNA-seq reads for each library were mapped and quantified independently using reference transcriptome sequences of human genome build hg38, downloaded via RefSeq. Differentially expressed genes from RNA-Seq data were detected using the method of Kallisto. From the mapped sequences,

the number of reads per annotated genes were counted using Tximport. The TPM values of the *Negr1* gene were compared.

QUANTIFICATION AND STATISTICAL ANALYSIS

Statistics

All quantitative data are expressed as means ± SEM. Differences were determined by unpaired Student's t-test or one-way analysis of variance test with genotype of tissue by the least significant difference post-hoc test and were considered significant when p was less than 0.05. Data were analyzed using SPSS version 23 software (IBM, Armonk, NY, USA).